

Sensor And Simulation Notes

Note 344

21 June 1992

Accuracy Considerations in the  
Design of B-Dot and I-Dot Sensors

Carl E. Baum

Phillips Laboratory

Abstract

In the design of B-dot and I-dot sensors with calculable sensitivities, accurate realization of the desired calculable geometries is important. This paper summarizes various useful accuracy bounds and estimates that one can use to make the errors often quite small. These include the perturbations due to non-zero thickness metal sheets and non-zero radius of signal-cable shields.

CLEARED  
FOR PUBLIC RELEASE

PL/PA 12AUG 92

PI 92-0570

## I. Introduction

In designing electromagnetic-field sensors one is concerned with the question of accuracy. How well does one know the relationship between the electromagnetic field (or its time derivative) and some voltage or current delivered to some terminal into some specified impedance? Here we are considering passive geometric structures (antennas) which (among other things) have accurately calculable quasi-static response parameters. Given the basic parameters in the constitutive equations ( $\mu_0$  by definition,  $\epsilon_0$  from the speed of light  $c$  known to many significant figures), then with the Maxwell equations one can design some such sensors that are "calibratable by a ruler" [16].

One can, of course, expose the sensor to some standard field, current, etc., but this begs the question. What calibrates the calibrator? This is some device which establishes an electromagnetic-field configuration when driven (at one or more terminals) by electrical source(s). A fundamental electromagnetic principle here is reciprocity which relates the response of antennas in transmission and reception (providing non-reciprocal media are not used, the typical case). The accuracy of the transmitting antenna (field producer) and sensor (field receiver) are comparable geometric (ruler) problems. If there is some disagreement between transmitter and receiver which one is in error? Perhaps both are in error. In principle it is no more difficult to make a standard sensor than a standard electromagnetic source. For both the use of special calculable geometries with error estimates for how well one realizes these geometries is essential.

Some previous papers have addressed some problems concerning the accuracy of electric or D-dot sensors, including the presence of dielectrics and non-zero thickness of conducting plates (e.g. ground planes) used in the design [4,5]. Similar calculations can be (and have been) used for the non-ideal conductors (cable shields, non-zero thickness metal shields, nearby metal scatterers) used in B-dot and I-dot sensors. This paper summarizes a number of these.

## II. Bounds on Loop Area

In calculating the equivalent area of a loop (magnetic-dipole) sensor one considers the case that the load impedance (resistive) is large enough that the magnetic flux is not excluded from the loop structure (open-circuit conditions). Then imagine as in Fig. 2.1 that one is looking along a symmetry axis of the loop (the z axis), this axis being parallel to the component of the magnetic field one is measuring. By use of symmetry planes in the design one can accurately assure that the equivalent area and open-circuit voltage are described by [16]

$$\vec{A}_{eq} = A_{eq} \vec{1}_z, V_{o.c.} = \vec{A}_{eq} \cdot \frac{\partial \vec{B}^{(inc)}}{\partial t} \quad (2.1)$$

In the example in Fig. 2.1, the sensor conductors have four symmetry planes (spaced at  $\pi/4$  angles) containing the symmetry axis and one symmetry plane perpendicular to the symmetry axis (parallel to the page). This is an example of  $D_{4,t}$  (dihedral) symmetry [12,13], as the intersection of the first four symmetry planes with the fifth gives four 2-fold rotation axes. Note that this symmetry applies to the exterior scattering, not the routing of the signals which occurs on cables that are made part of (bonded into) the overall structure. While this symmetry group is the basis for the usual MGL (multigap loop) design, various other choices are also used for other loop designs.

Referring to Fig. 2.1 let us write

$$NA_- \leq A_{eq} \leq NA_+ \quad (2.2)$$

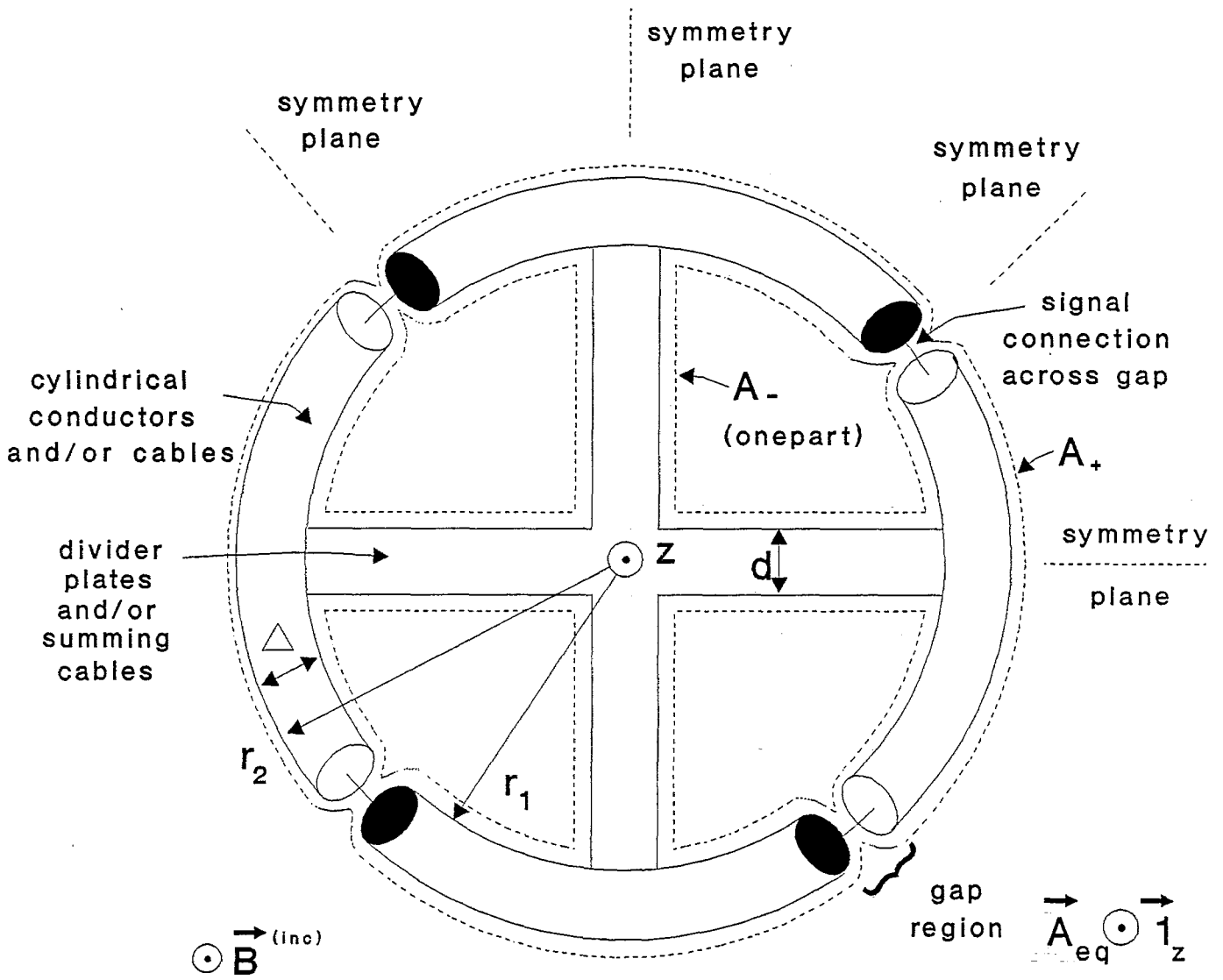
$N = \text{number of loop turns}$

where  $A_{eq}$  is taken as positive in (2.2). Here  $N$  can be an integer or even a fraction. The typical MGL full loop (not on a ground plane) has  $N = 1/2$  due to series/parallel connection of the signal from the four quadrants.

In establishing these bounds, note that (looking along the loop axis) the structure is sparse so that the z component of the magnetic field is negligibly perturbed. One can picture the magnetic field being locally distorted to pass on both sides of the conductors so that some path lying in the conductor represents an effective boundary for equivalent area purposes. Then the outermost perimeter gives  $A_+$  which is

$$A_+ = \pi r_2^2 \quad (2.3)$$

for a circular cylinder (radius  $r_2$ ) tightly circumscribing the sensor. Note that this can be reduced slightly as indicated in the gap regions if a wire comes out of a coaxial cable there. The example of the loop-gap connections is only illustrative as there are many other types [16]. Other formulas for  $A_+$  can be readily derived for non-circular-cylindrical loop designs.



View along direction of  $\vec{A}_{eq}$  (loop axis)  
 Thickness of plates exaggerated

Fig. 2.1 Loop-Area Estimates

For a lower bound we have

$$A_- = \pi r_1^2 - N_d r_1 d \quad (2.4)$$

$N_d$  = number of radial divider plates, cables, etc.  
 $d$  = maximum thickness of dividers.

The example in Fig. 2.1 has  $N_d = 4$ . If a half-loop version is built on a ground plane, then two of the dividers can be considered as part of the ground plane. Depending on design specifics, how much needs to be included in (2.4) depends on how much is raised above the surrounding ground plane, together with the image to put the result on a full-loop basis. Note that external dielectrics are not considered in this bounding, since they are readily penetrated by the magnetic field.

So one view of the sensor accuracy is to bring the upper and lower bounds in (2.2) close together and use as our estimate

$$A_{eq} = N \frac{A_+ + A_-}{2} \quad (2.5)$$

This minimizes the error as

$$(2.6) \quad \Delta A = N \frac{A_+ - A_-}{2}$$

$$\frac{\Delta A}{A_{eq}} = \frac{A_+ - A_-}{A_+ + A_-}$$

Choosing some desirable value of  $A_{eq}$  (e.g.  $1.00 \times 10^{-2} \text{ m}^2$ ) then one can equally space  $A_+$  and  $A_-$  above and below  $A_{eq}$ . The remaining error as in (2.6) can be made quite small, at least for large loops, say a percent or so. If the divider plates can be neglected we have

$$A_+ - A_- = \pi (r_2^2 - r_1^2) = 2\pi \Delta \frac{r_2 + r_1}{2}$$

$$A_+ + A_- = \pi (r_2^2 + r_1^2) = 2\pi \left[ \frac{r_2 + r_1}{2} \right]^2$$

$$\frac{\Delta A}{A_{eq}} = \Delta \left[ \frac{2}{r_2 + r_1} \right] \quad (2.7)$$

$$\Delta = r_2 - r_1$$

So as one would expect the relative error is proportional to the ratio of the conductor thicknesses to the loop dimension.

So far the discussion has concerned the loop conductors as perfectly conducting and thereby excluding magnetic flux. In the low-frequency limit magnetic fields penetrate real conductors, giving another way to view the equivalent area. In this case the wires (center conductors) inside the cables define (at least in part) the perimeter for the equivalent area. Ideally one would like this estimate of the equivalent area to agree closely with the previous estimate in (2.5). With such wires enclosed in cables (or as strip lines) included in the regions of  $A_+$  but not  $A_-$ , in Fig. 2.1, this agreement is assured at least in the bounding sense of (2.2). However, by judicious positioning of these signal wires within the ambiguity area one can try to make the low-frequency estimate correspond closely to that in (2.5), or to more accurate estimates discussed later in this paper.

### III. Bounds on Mutual Inductance

The same concepts can be adapted for I-dot sensors. As in Fig. 3.1 consider the sensor as a collection (distribution) of loops in planes of constant  $\phi$  which respond to  $B_\phi$  averaged over  $0 \leq \phi \leq 2\pi$ . There are various forms of winding such loop ensembles, including parallel forms for good high frequency performance [3]. Assuming an axially symmetric current distribution in the z direction, such as a wire with current I on the z axis, we have the quasi-static magnetic field

$$B_\phi = \mu_o H_\phi = \frac{\mu_o I}{2\pi \Psi} \quad (3.1)$$

$(\Psi, \phi, z) = \text{cylindrical coordinates}$

Note that the permeability of free space  $\mu_o$  is used since the sensor is assumed to have an air core. A magnetic core is more appropriate for short-circuit conditions (due to large inductance).

The open circuit voltage is

$$V_{o.c.} = M \frac{\partial I}{\partial t} \quad (3.2)$$

$M = \text{mutual inductance}$

$$M = N \frac{\mu_o W}{2\pi} \ln \left( \frac{r_2}{r_1} \right)$$

$N = \text{number of loop turns}$

Here  $r_1$ ,  $r_2$ , and  $w$  are effective dimensions with upper (+) and lower (-) bounds as indicated in Fig. 3.1. For the rectangular cross section (plane of constant  $\phi$ ) we have the bounds

$$\frac{\mu_o W_-}{2\pi} \ln \left( \frac{r_{2+}}{r_{1+}} \right) \leq \frac{M}{N} \leq \frac{\mu_o W_+}{2\pi} \ln \left( \frac{r_{2+}}{r_{1-}} \right) \quad (3.3)$$

As in the previous section, these bounding dimensions include all the cabling and conductors. The bounds define a toroid-like object (except for typically rectangular cross section), i.e. a bounding body of revolution with respect to the z axis. The bounds can be slightly tightened by accounting for the loop-gap region where one has an annular slot (constant  $\Psi, z$ ) with signal wires crossing the slot. In principle, one can also have divider plates as bodies of revolution (e.g. parallel to a plane of constant z). These would be included by appropriate reduction of the lower bound (analogous to the previous section).

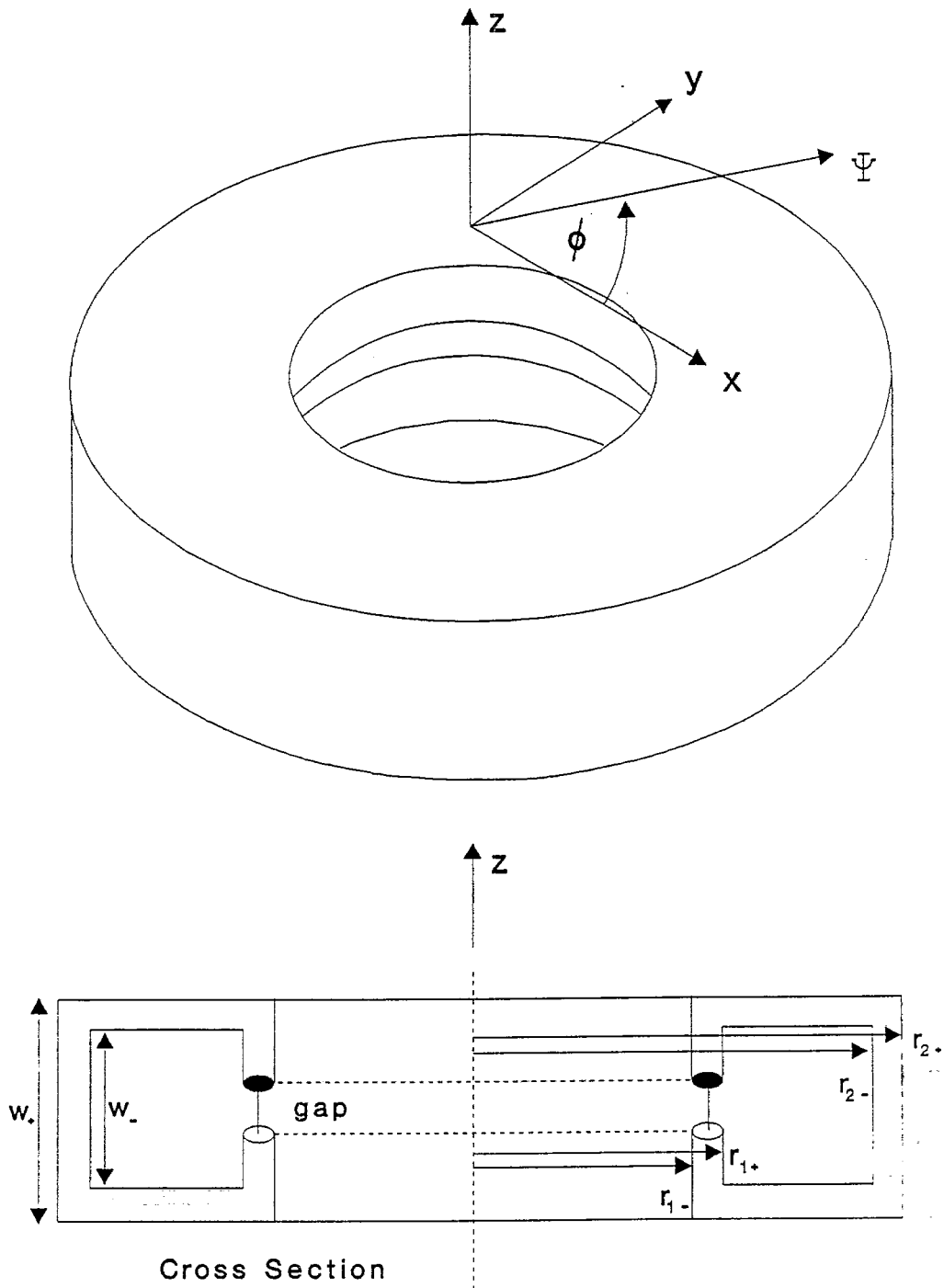


Fig. 3.1 I-dot Sensor Geometry

So one can use as the estimate of M

$$\begin{aligned}
 M &= N \frac{\mu_o}{4\pi} \left\{ w_+ \ln \left( \frac{r_{2+}}{r_{1-}} \right) + w_- \ln \left( \frac{r_{2-}}{r_{1+}} \right) \right\} \\
 &\approx N \frac{\mu_o}{2\pi} w \ln \left( \frac{r_2}{r_1} \right) \\
 w &= \frac{w_+ + w_-}{2} \tag{3.4} \\
 r_1 &= \sqrt{r_{1+} r_{1-}} \\
 r_2 &= \sqrt{r_{2+} r_{2-}}
 \end{aligned}$$

This minimizes the error as

$$\begin{aligned}
 \Delta M &= N \frac{\mu_o}{4\pi} \left\{ w_+ \ln \left( \frac{r_{2+}}{r_{1-}} \right) - w_- \ln \left( \frac{r_{2-}}{r_{1+}} \right) \right\} \\
 &\approx N \frac{\mu_o}{4\pi} \left\{ [w_+ - w_-] \ln \left( \frac{r_2}{r_1} \right) \right. \\
 &\quad \left. + w \left[ \ln \left( \frac{r_{2+}}{r_{2-}} \right) + \ln \left( \frac{r_{1+}}{r_{1-}} \right) \right] \right\} \tag{3.5}
 \end{aligned}$$

Choosing some desirable value for M (e.g. 2.00 nH), then one can choose the sensor dimensions with the bounds spaced equally above and below. The remaining error can be made quite small, at least for large sensors.

The foregoing discussion has been applied in the design of the CPM (cylindrical parallel mutual-inductance) type of sensor. However, if the frequency is high enough that skin depths can be neglected, and if the space between inner and outer dimensions is "completely" filled with metal (except in the gap region) with signal cables contained in the metal, then the formula

in (3.1) applies within the internal dimensions which can now be used to give

$$M = N \frac{\mu_o}{2\pi} w_{\ell} \ln \left( \frac{r_{2-}}{r_{1+}} \right) \quad (3.6)$$

with a correction depending on the exact position the signal conductors emerge from coaxial cables to cross the gap. This is the appropriate approximation for use with the IMM, OMM, and FMM sensors [16].

Another source of error concerns the lack of rotation symmetry in the magnetic field as in (3.1) such as by a current not centered on the z axis. One can make a fourier expansion of  $B_{\phi}$  with  $\cos(n\phi)$  and  $\sin(n\phi)$  terms. The previous discussion applies to the  $n = 0$  term. For higher order terms one can cancel out the first several of these by sampling the field at  $N_{\phi}$  positions spaced in  $2\pi/N_{\phi}$  increments of the angle  $\phi$  around the sensor. The first contributing term (to the error) comes from  $n = N_{\phi}$ . By moving the wire off the z axis (but still parallel to the z axis) one can determine for a particular sensor how close one can approach the sensor structure for a given allowed change (error) in the sensor output.

At high frequencies there is a certain ambiguity concerning how to think about the sensor response. The form in (3.1) is a simplification of

$$\begin{aligned} \nabla \times \vec{H} &= \vec{J} + \frac{\partial D}{\partial t} = \vec{J} + \epsilon_o \frac{\partial \vec{E}}{\partial t} = \vec{J}_t \\ \int_C \vec{H} \cdot d\vec{l} &= \int_S \vec{J}_t \cdot d\vec{S} \\ \int_0^{2\pi} B_{\phi} d\phi &= \mu_o \int_0^{2\pi} H_{\phi} d\phi = \frac{\mu_o}{\Psi} \int_S \vec{J}_t \cdot \vec{l}_z dS \end{aligned} \quad (3.7)$$

where the contour C is along a circle of constant  $(\Psi, z)$  bounding the circular disk on constant z with unit normal  $\vec{l}_z$ . So the sensor, by integrating the magnetic field around a closed contour, measures the enclosed total current (including displacement). This is then a matter of definition. If one wishes the current on a small wire (compared to  $r_{1-}$ ), there are potential high-frequency errors (depending on details of the incident fields). On the other hand, one may design a measurement around the total current density, as in the case of the FMM [16], in which the view in (3.7) is more appropriate for defining the sensor response.

#### IV. Approximation of Thick Conducting Sheet by Ellipsoid

In passing around divider plates as in Fig. 2.1, the magnetic field is changed in value near the plates. This enhancement of the magnetic field can be estimated via the canonical problem in Fig. 4.1. Here an ellipsoid with  $d \ll a, b$  is used to approximate such a plate of thickness about  $2d$ . This also applies to the case of a ground plane of thickness  $d$  mounted on a large (perfectly) conducting plate on the  $z = 0$  plane. Here we are concerned with the magnetic field at

$$(x, y, z) = (0, 0, d) \quad (4.1)$$

The incident magnetic field of strength  $B_0$  is taken in the  $x$  direction with symmetry making the total field just outside the ellipsoid at the point in (4.1) parallel to the incident field.

This enhancement factor has been derived in [9] as

$$f_H = \frac{B_x}{B_0} = \begin{cases} 1 + \frac{db}{a^2 - b^2} \left[ K \left( 1 - \left( \frac{b}{a} \right)^2 \right) - E \left( 1 - \left( \frac{b}{a} \right)^2 \right) \right] & \text{for } a > b \\ 1 + \frac{da}{b^2 - a^2} \left[ \left( \frac{b}{a} \right)^2 E \left( 1 - \left( \frac{a}{b} \right)^2 \right) - K \left( 1 - \left( \frac{a}{b} \right)^2 \right) \right] & \text{for } b > a \\ 1 + \frac{\pi}{4} \frac{d}{a} \quad (a = b, \text{ flat oblate spheroid}) & \end{cases} \quad (4.2)$$

where the argument of the complete elliptic integrals is the parameter  $m$  as in [14]. For comparison, the enhancement factor for an electric field in the  $z$  direction is  $1 + \pi d / (2a)$  (for small  $d/a$ ) for an oblate spheroid ( $a = b$ ) [5,9]. So the fractional increase of the magnetic field is only half that of the electric field in this case.

Additional limiting cases are

$$f_H = 1 \text{ for } \frac{a}{b} \rightarrow \infty \text{ (independent of } d/b) \quad (4.3)$$

(elliptic cylinder along  $x$  axis)

$$f_H = 1 + \frac{d}{a} \text{ for } \frac{b}{a} \rightarrow \infty \text{ (elliptic cylinder along } y \text{ axis)}$$

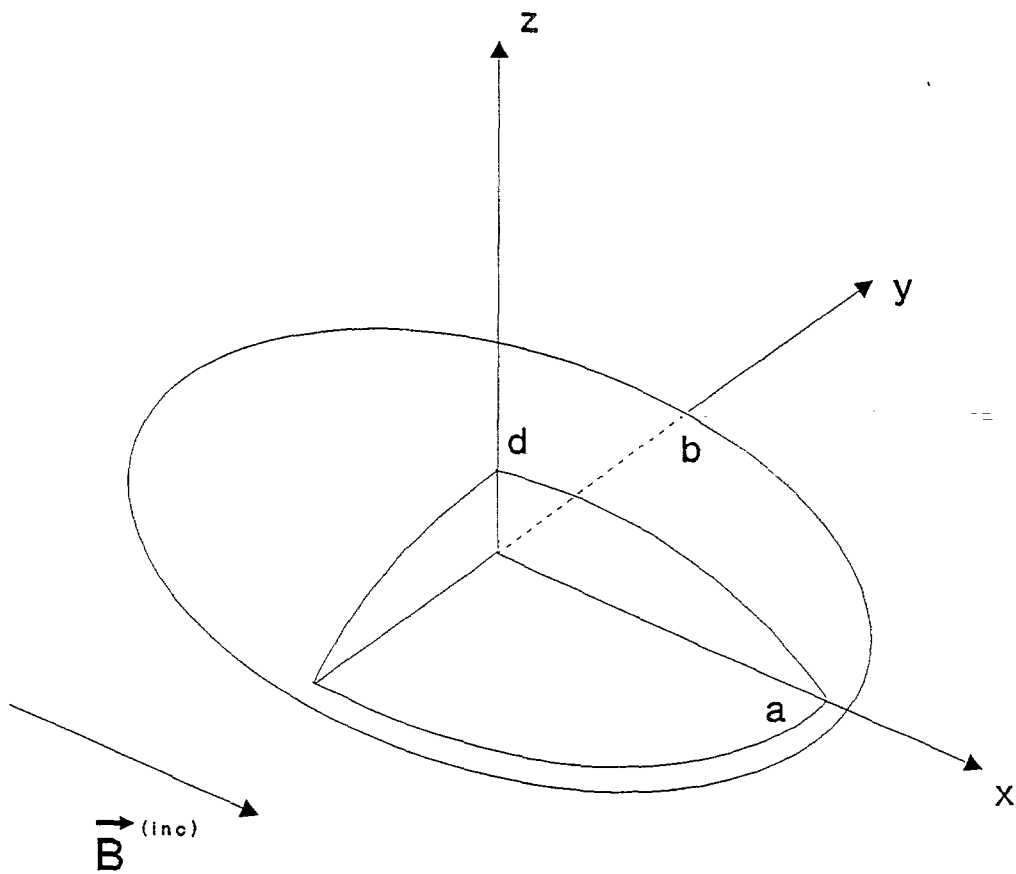


Fig. 4.1 Ellipsoidal Model of Divider Plates and Ground Plane

In the first of these there is no enhancement (field parallel to the elliptic cylinder), while in the second case there is still an enhancement.

These enhancement factors can be used to obtain more accurate estimates of equivalent area in section II. For  $d, b \ll a$  the enhancement can be quite small. This is a guideline then for sensor ground planes (which in turn are mounted on large conducting surfaces). Make the plate thin, but long in the magnetic-field direction.

When used as a divider plate as in Fig. 2.1, the enhancement is again small provided  $d \ll a$ . Even with this enhancement one can estimate the equivalent area more accurately by taking  $A_0$  and increasing it by the enhancement factor. Note that there may be more than one such divider plate, as well as curved cylindrical plates (axis parallel to magnetic field), as part of the loop structure. However, this view of magnetic field enhancement only applies for skin depths  $\ll d$ .

V. Approximation of Finite-Length Conducting Circular Cylinder by Prolate Spheroid: Magnetic Field Parallel to Major Axis

Another application of the ellipsoidal scattering model concerns a circular cylindrical scatterer which would be on the loop axis (as in Fig. 2.1). This finite-length conducting tube may be part of the mechanical structure of the loop (anchoring the divider plates), as well as serving as a conduit for signal cables leaving along the loop axis to recording instruments or data telemetry units. In this case let us set  $d = b$  in Fig. 4.1 and consider again the magnetic field enhancement as in (4.1).

From [9] one uses for the prolate spheroid

$$f_H = \frac{H_x}{H_o} = \frac{N_a}{N_a - 1} \rightarrow 1 + \left(\frac{b}{a}\right)^2 \left[ \ln\left(\frac{2a}{b}\right) - 1 \right] \quad (5.1)$$
$$\text{as } \frac{b}{a} = \frac{d}{a} \rightarrow 0$$

So the increase in the magnetic field is quite small, not quite quadratic in  $b/a$ .

There is also the case that one has what can be approximated as a semi infinite cylinder. This corresponds to the sensor near the end of a boom which contains the signal cables. This is treated for a particular shape near the cylinder end in [6,11].

VI. Change of Magnetic Flux by Conducting Circular Cylinder: Field Perpendicular to Axis

Consider now cables with axis transverse to the incident magnetic field as in Fig. 6.1. These may appear in various places in the overall geometry of Figs. 2.1 and 3.1. Here we take

$$\begin{aligned}\vec{B}^{(inc)} &= B_o \vec{i}_y = B_o [\sin(\phi) \vec{i}_\Psi + \cos(\phi) \vec{i}_\Phi] = \nabla \Phi_m^{(inc)} \\ \Phi_m^{(inc)} &= B_o y = B_o \Psi \sin(\phi)\end{aligned}\quad (6.1)$$

for the incident magnetic field. The total field is

$$\begin{aligned}\vec{B} &= \vec{B}^{(inc)} + \vec{B}^{(sc)} \\ \Phi_m &= \Phi^{(inc)} + \Phi^{(sc)}\end{aligned}\quad (6.2)$$

The scattered field is found in the usual way from the solution for the Laplace equation (for  $\Psi > \Psi_o$ ) as

$$\begin{aligned}\Phi^{(sc)} &= B_o \Psi_o^2 \Psi^{-1} \sin(\phi) = B_o \left(\frac{\Psi_o}{\Psi}\right)^2 y \\ \vec{B}^{(sc)} &= \nabla \Phi^{(sc)} = -B_o \left(\frac{\Psi_o}{\Psi}\right)^2 \sin(\phi) \vec{i}_\Psi + B_o \left(\frac{\Psi_o}{\Psi}\right)^2 \cos(\phi) \vec{i}_\Phi\end{aligned}\quad (6.3)$$

which gives the boundary condition of zero normal magnetic field at the surface of the perfectly conducting cylinder of radius  $\Psi_o$ .

The magnetic field at the cylinder surface at  $\phi = 0, \pi$  is twice the incident field. However, this value is not appropriate for correcting the equivalent area (via  $A_{eq}$ ) or mutual inductance. In going out from the cylinder to a position on the x axis consider  $A'_{eq}(x)$  as the magnetic flux intercepted per unit of incident field and per unit of cable length (z direction) as

$$\begin{aligned}A'_{eq}(x) &= \frac{1}{B_o} \int_{\Psi_o}^x \vec{i}_y \cdot \vec{B} \Big|_{y=0} dx' \\ &= \int_{\Psi_o}^x \left[ 1 + \left(\frac{\Psi_o}{x'}\right)^2 \right] dx' \\ &= \left[ x' - \frac{\Psi_o^2}{x'} \right]_{\Psi_o}^x \\ &= x \left[ 1 - \left(\frac{\Psi_o}{x}\right)^2 \right]\end{aligned}\quad (6.4)$$

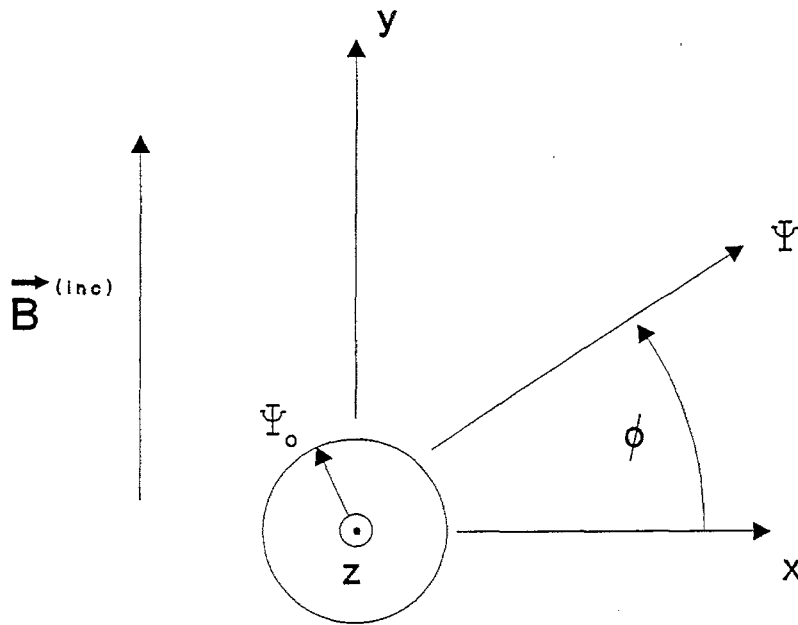


Fig. 6.1 Distortion of Magnetic Field Transverse to Axis of Perfectly Conducting Cylinder

Comparing this to the result for a very thin cable we have

$$\frac{A_{eq}(x)}{A_{eq}(x) | \Psi_o = 0} = 1 - \left( \frac{\Psi_o}{x} \right)^2 \quad (6.5)$$

So the error is  $-(\Psi_o/x)^2$  which can be quite small if  $x$  is say ten times the cable radius. So as long as the other conductors are sufficiently far from the cable (which might also include a conducting sheet on the  $x = 0$  plane (except inside the cable)), the error (or correction) in equivalent area can be made acceptably small.

## VII. Equivalent Spacing of Two Parallel Conducting Circular Cylinders

The proximity of a second cable to the first (as in section VI) can be considered via two parallel perfectly conducting cylinders as in Fig. 7.1. Here, two cylinders of radius  $\Psi_0$  are spaced a distance  $h$  between centers. The incident magnetic field is the same as in section VI, and the question concerns how much magnetic flux passes between the two cylinders. This is given by the equivalent area per unit length, or equivalent height, as

$$h_{eq} = A_{eq} = \frac{1}{B_0} \int_{-\frac{h}{2} + \Psi_0}^{\frac{h}{2} - \Psi_0} \vec{i}_y \cdot \vec{B} |_{y=0} dx \quad (7.1)$$

Noting reciprocity between transmission and reception, this has the well-known solution [1]

$$\begin{aligned} h_{eq} &= 2 \left[ \left( \frac{h}{2} \right)^2 - \Psi_0^2 \right]^{\frac{1}{2}} \\ &= h \left[ 1 - 2 \left( \frac{\Psi_0}{h} \right)^2 + \mathcal{O} \left( \left( \frac{\Psi_0}{h} \right)^4 \right) \right] \quad \text{as } \frac{\Psi_0}{h} \rightarrow 0 \end{aligned} \quad (7.2)$$

Comparing this to (6.4) note the similar form with the correction proportional to  $(\Psi_0/h)^2$ . However, (7.2) takes account of the mutual interaction of the two cylinders, thereby being more accurate for such a case.

Note that  $x = 0$  is a symmetry plane on which one can place a perfectly conducting sheet. So the results here also apply to the case of a single cylinder centered a distance of  $h/2$  from a conducting plate.

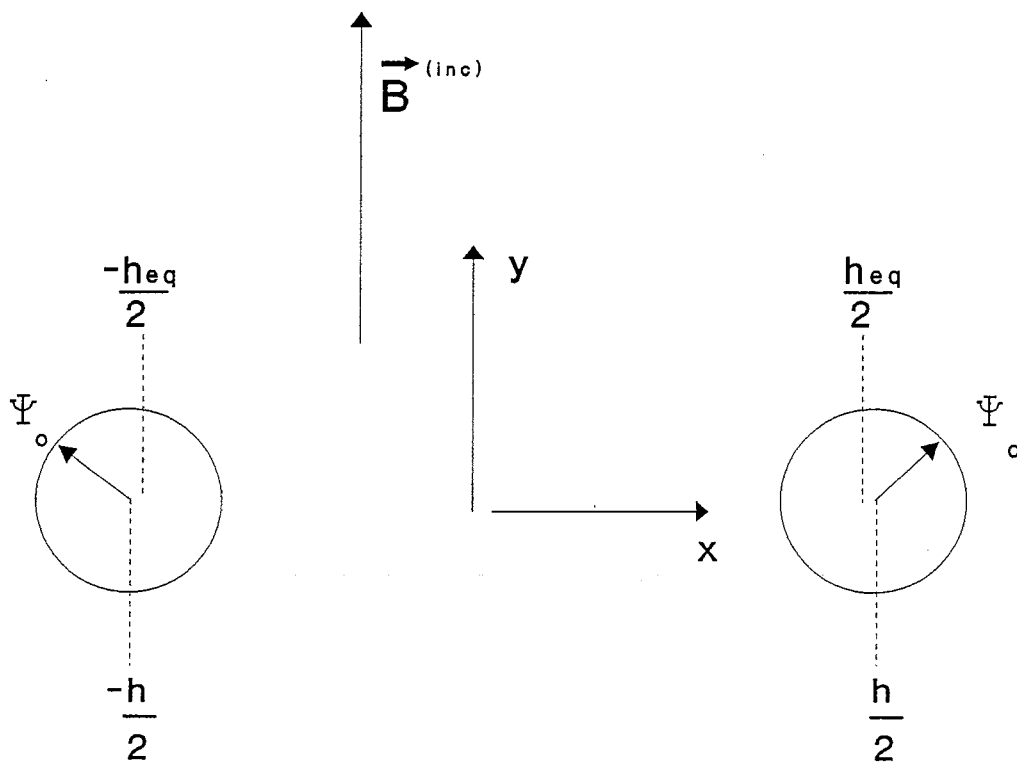


Fig. 7.1 Magnetic-Flux Interception by Two Parallel Perfectly Conducting Cylinders

## VIII. Effect of Nearby Scatterers

Associated with the sensor are often nearby scatterers such as cable connectors, baluns, data telemetry devices, etc. These may appear at the end of some cable and possibly be mounted on some ground plane or sheet of metal on a symmetry plane associated with the sensor.

A simple way to think of the errors introduced by such scatterers is in terms of the quasi-static magnetic field, which for distance  $r$  large compared to some dimension  $r_0$  of the scatterer can be treated in terms of a magnetic polarizability tensor  $\vec{M}$  [7,15] where

$$\begin{aligned}\vec{m} &= \vec{M} \cdot \vec{H}^{(inc)} \quad (\text{magnetic dipole moment}) \\ \vec{H}^{sc} &= \frac{1}{4\pi r^3} [3\vec{1}_r \vec{1}_r - \vec{1}] \cdot \vec{m} \\ &= \frac{1}{4\pi r^3} [3\vec{1}_r \vec{1}_r - \vec{1}] \cdot \vec{M} \cdot \vec{H}^{(inc)}\end{aligned}\tag{8.1}$$

The polarizability is of the order of the volume of the scatterer (i.e.  $r_0^3$ ), so the scattered field goes like  $(r_0/r)^3$ . Note that this is a quasistatic approximation, and that as frequency is increased so that the radian wavelength  $\lambda$  becomes of the order of  $r$  or less there are other terms ( $r^{-2}$  and  $r^{-1}$ ) that come into play.

A simple shape for approximating such a scatterer is a sphere of radius  $r_0$  for which we have [9]

$$\begin{aligned}\vec{M} &= -\frac{3}{2} \text{Volume} = -2\pi r_0^3 \\ \vec{H}^{(sc)} &= -\frac{3}{8}\pi \left(\frac{r_0}{r}\right)^3 [3\vec{1}_r \vec{1}_r - \vec{1}] \cdot \vec{H}^{(inc)}\end{aligned}\tag{8.2}$$

with the coefficient in this last formula giving the relative error introduced in the field. This can be refined by using ellipsoidal or other shapes with known magnetic polarizability.

Note that dielectric scatterers are not significant perturbers of quasi-static magnetic fields. They do, however, perturb quasi-static electric fields and so are significant in the case of electric sensors via their electric polarizability [4]. For magnetic sensors it is the magnetic polarizability of highly conducting or permeable scatterers that is significant.

## IX. Concluding Remarks

Besides these simple formulas that can be used to estimate or bound equivalent areas and mutual inductance, there are other considerations in the design of accurate magnetic-based sensors [16]. For example, in multiturn loops one can alternate the crossovers (in an over/under sense) of the conductors (sometimes coaxial or even triaxial cables) [2,8]. The incident magnetic field may not be uniform if one is making measurements near conductors. In such a case one can use special geometries to minimize the error [2,10].

Note that here we have been considering the open-circuit parameters  $\bar{A}_{eq}$  and  $M$  which are related to interception of magnetic flux. Short-circuit parameters bring in the self inductance of the sensor, a parameter which is usually more difficult to accurately calculate.

## References

1. C. E. Baum, Impedances and Field Distributions for Symmetrical Two Wire and Four Wire Transmission Line Simulators, Sensor and Simulation Note 27, October 1966.
2. C. E. Baum, Some Considerations for Electrically-Small Multi-Turn Loops, Sensor and Simulation Note 43, May 1967.
3. C. E. Baum, Some Considerations for Inductive Current Sensors, Sensor and Simulation Note 59, July 1968.
4. C. E. Baum, The Circular Parallel-Plate Dipole, Sensor and Simulation Note 80, March 1969.
5. C. E. Baum, Further Considerations for the Circular Parallel-Plate Dipole, Sensor and Simulation Note 86, June 1969.
6. R. W. Latham and K. S. H. Lee, Magnetic-Field Distortion by Specific Axisymmetric, Semi-Infinite, Perfectly Conducting Body, Sensor and Simulation Note 102, April 1970.
7. C. E. Baum, Some Characteristics of Electric and Magnetic Dipole Antennas for Radiating Transient Pulses, Sensor and Simulation Note 125, January 1971.
8. C. E. Baum, Further Considerations for Multiturn Cylindrical Loops, Sensor and Simulation Note 127, April 1971.
9. K. S. H. Lee, Electrically-Small Ellipsoidal Antennas, Sensor and Simulation Note 193, February 1974.
10. C. E. Baum, Idealized Electric- and Magnetic-Field Sensors Based on Spherical Sheet Impedances, Sensor and Simulation Note 283, March 1983, and Electromagnetics, 1989, pp. 113-146.
11. D. V. Giri and C. E. Baum, Airborne Platform for Measurement of Transient or Broadband CW Electromagnetic Fields, Sensor and Simulation Note 284, May 1984, and Proc. AICWEMC, Bangalore India, 1985, pp. 79-82, and Electromagnetics, 1989, pp. 69-84.
12. D. V. Giri and C. E. Baum, High-Frequency Capacitors, Energy Storage and Dissipation Note 10, March 1990.
13. C. E. Baum and H. N. Kritikos, Symmetry in Electromagnetics, Physics Note 2, December 1990.
14. M. Abramowitz and I. A. Stegun (eds.), Handbook of Mathematical Functions, AMS-55, U.S. Government Printing Office, 1964.
15. K. S. H. Lee (ed.), EMP Interaction: Principles, Techniques, and Reference Data, Hemisphere Publishing Corp., 1986.
16. C. E. Baum, Electromagnetic Sensors and Measurement Techniques, pp. 73-144, in J. E. Thompson and L. H. Leussen, Fast Electrical and Optical Measurements, Martinus Nijhoff, Dordrecht, 1986.